

## Shaking table testing of an innovative wireway vibration attenuation system



Han V. Tran <sup>a</sup>, Sung Chan Kim <sup>b</sup>, Jiuk Shin <sup>c</sup>, Kihak Lee <sup>a,\*</sup>

<sup>a</sup> Deep Learning Architecture Research Center, Department of Architectural Engineering, Sejong University, 209 Neungdong-ro, Gwangjin-gu, Seoul 05006, Republic of Korea

<sup>b</sup> Sehong Inc, Ltd, 16, Tapsil-ro 58, Giheung-gu, Yongin-si, Gyeonggi-do 17084, Republic of Korea

<sup>c</sup> Department of Architectural Engineering, Gyeongsang National University, Jinju-daero, Jinju-si, Gyeongsangnam-do 52828, Republic of Korea

### ARTICLE INFO

#### Keywords:

Wireway  
Shaking table test  
Friction damper  
Non-structural components  
Vibration attenuation

### ABSTRACT

The seismic performance of the lighting systems is rarely reported in the literature, although previous studies indicate that they could be vulnerable during an earthquake. This study investigated the effect of various connectors on the seismic performance of an innovative wireway vibration attenuation system for raceway light fixtures using shaking table tests based on ICC-ES AC156 standard. The floor spectrum was created, and its compatible floor motion time history was employed as the input motion. Four typical prototypes were prepared with connectors suitable for mounting on a variety of structural components, including ceiling, H-beam frame, wall, and beam and column. The test results demonstrated that the specimens with the direct connectors (Wall and H-beam frame) had excellent seismic performance, 1.4–2.0 times higher than those with the pole connectors (Ceiling and Beam-column). Therefore, the direct connectors are proposed for this innovative system to decrease the danger of system failure during an earthquake.

### 1. Introduction

Non-structural components (NSCs) are those systems and components attached to floors, roofs, and walls of a building or industrial facility that are not part of the main load-bearing structural systems but may also be subjected to significant seismic actions [1]. The Federal Emergency Management Agency (FEMA) E-74 [2] categorized NSCs into three major categories: (1) the architectural components, (2) the mechanical, electrical, and plumbing systems and (3) the furniture, fixtures, equipment, and other contents of the NSCs.

Reports from past earthquakes indicate that the majority of damage occurred as a result of the destruction and collapse of NSCs, rather than the collapse of main structures. The research by Kircher and Filiatrault [3,4] showed that economic losses associated with the failure of NSCs during an earthquake, including property loss, site clean-up, and replacement expenses, much outweigh structural damage losses. For instance, during the 1989 Loma Prieta earthquake, it was stated that the suspended ceilings and lighting systems of San Francisco International Airport suffered major damage [5,6]. After the 1994 Northridge earthquake in Los Angeles [1], damage to severe emergency power systems at a key local hospital was reported. The 1985 Mexico Earthquake and the

2010 Haiti Earthquake seriously damaged electrical cabinets at critical facilities [2]. Electrical systems in major public buildings in South Korea, including hospitals, Korea train express (KTX) railway stations, and shopping malls, degraded following the 2016 Gyeongju and 2017 Pohang earthquakes [7]. The damage of cladding panels was the most common in precast structures in the 2012 Emilia earthquake [8]. Similarly, reports of massive damage caused by the collapse of NSCs were also found in the following earthquakes: 2010 Chile [9], 2011 Christchurch, New Zealand [10], 2011 Tohoku-Oki, Japan [11], 2013 Lushan, China [12], 2016 Kumamoto, Japan [13], and 2016 Central Italy [14]. As a result, studies of seismic behavior of NSCs are widely recognized as a critical component of earthquake risk mitigation.

Over the last decade, the topic of increasing the seismic performance of NSCs has garnered considerable academic attention. Numerous studies, including dynamic testing of suspended ceiling systems [15–23], investigation of the seismic behavior of partition walls [16–18,24–27,22,28–32] and seismic response of facade walls and cladding panels [17,26,22,28,29,33], have been done to evaluate the seismic performance of the non-structural architectural components. The seismic performance of different equipment in laboratories and hospital facilities was described in [34–38].

\* Corresponding author.

E-mail address: [kihaklee@sejong.ac.kr](mailto:kihaklee@sejong.ac.kr) (K. Lee).

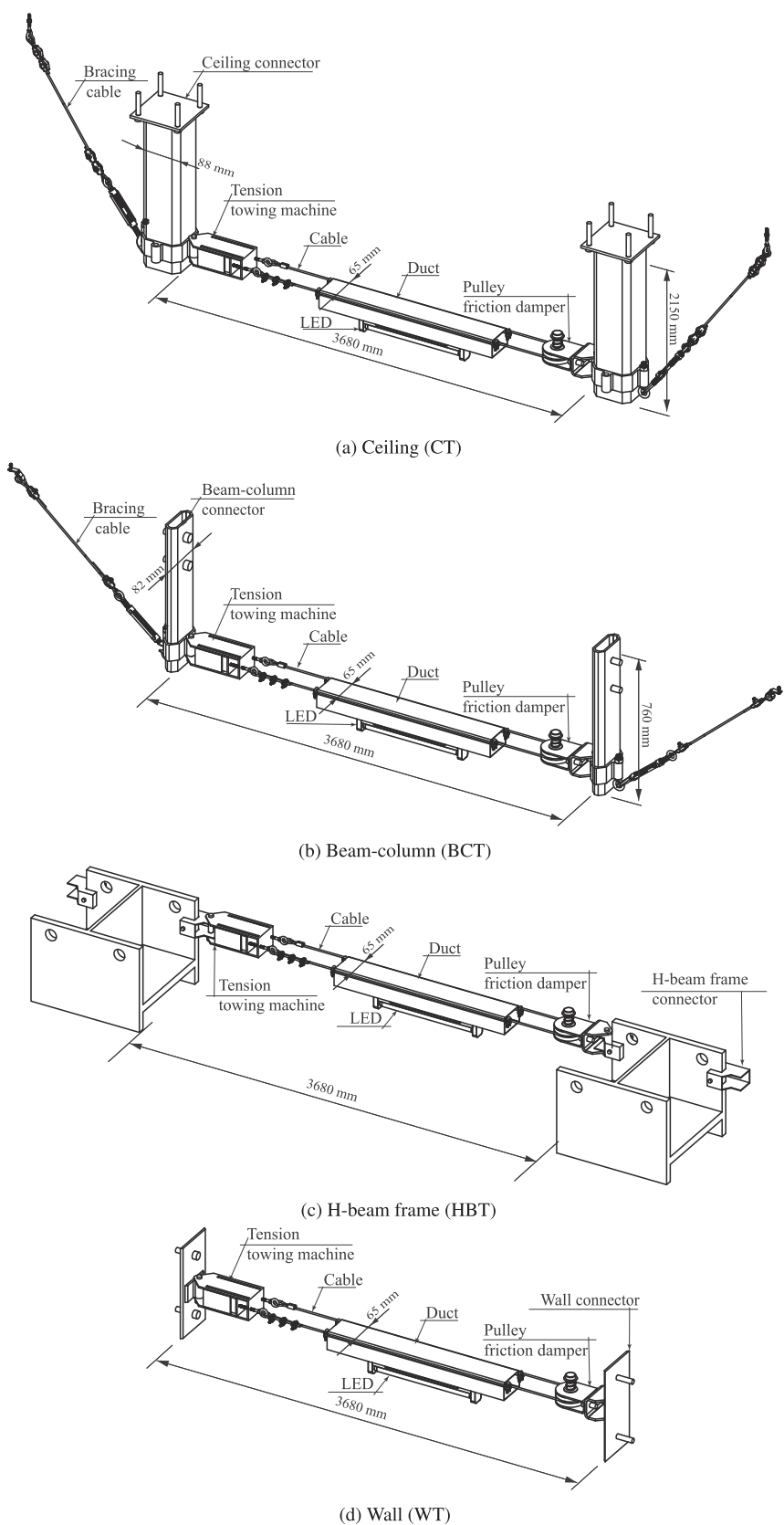


**Fig. 1.** Details of the four test specimens.

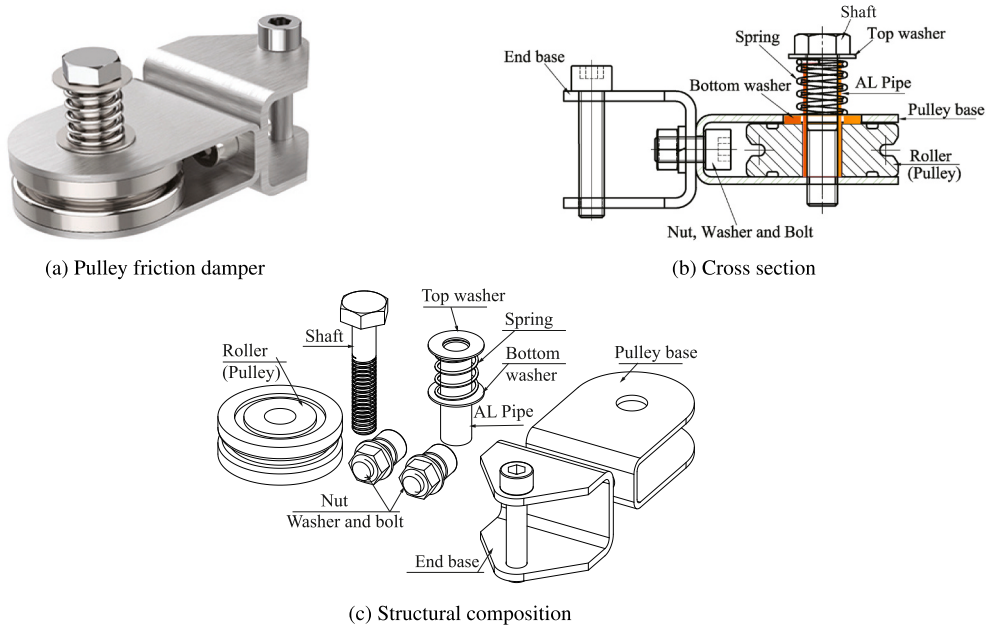


Fig. 2. Details of the pulley friction damper.

**Table 1**  
Mechanical characteristics of the cable.

Item	value	units
Wire structure	7 × 7	–
Diameter	4	mm
Maximum load bearing	9.8	kN
Weight per unit length	0.066	kg/m
Displacement (50 kgf tensile load)	0.7	mm
Modulus of elasticity	96,105	MPA

Meanwhile, several studies have focused on the seismic performance of non-structural electric components. Hwang et al. [39] used actual earthquake damage data to conduct a seismic fragility analysis of electrical equipment in a typical electric substation in the eastern United States. Porter et al. [40] evaluated the fragility of many types of electrical equipment that are frequently found in commercial and industrial buildings. Son et al. [41] conducted shaking table tests for the seismic qualification of an electrical cabinet. The study showed that the seismic response of a cabinet system during high frequency earthquakes is greater than its seismic response during low frequency earthquakes. Dinh et al. [42] performed an experimental seismic investigation of a 1000 kVA cast resin-type hybrid mold transformer using a tri-axial shaking table test. The test findings revealed that the damaged specimen was mostly caused by the slipping of certain gaskets and the loosening of the connecting bolts between the bed beam and the bottom beam. Wang et al. [43] investigated the seismic performance of a prototype diesel generator with a restrained vibration isolation system by conducting quasi-static cyclic loading tests and shaking table tests. The results of the tests revealed that the failure mechanisms of the restrained isolators were significant fatigue damage to the connection between the vertical restraint rods and the top plate, as well as pull-out failure of the

vertical restraint rods. The displacement response of the vibration isolation system could be lowered by incorporating snubbers into the system.

Until now, relatively few studies have been carried out on improving the seismic performance of lighting systems, which are an essential category of non-structural electrical components in buildings. Han et al. [44] proposed a novel lighting support system reinforced with a pulley friction damper, an innovative wireway vibration attenuation system for raceway light fixtures. The results of shaking table tests showed that their proposed friction dampers successfully reduced the seismic energy and peak oscillation in the lighting support systems, indicating that the novel system has the potential to become an attractive alternative earthquake-resistant for the building's conventional lighting systems.

It is noted that the novel lighting systems are connected to the main load-bearing components of the structure, such as walls, beams, columns, and floors, via a variety of connectors in actual practice. However, the previous research has not addressed the influence of these connectors on the system's earthquake performance. Therefore, a systematic study analyzing the effect of the connectors on the seismic performance of the novel systems is much needed.

In this paper, the seismic performance of such an innovative wireway vibration attenuation system for raceway light fixtures is experimentally investigated. Shaking table tests are conducted to ensure compliance with the ICC-ES AC156 standard [45]. The effect of various connectors of the system on the seismic performance are discussed. The following sections detail the experimental outcomes.

## 2. Shaking table test

### 2.1. Description of the test specimens

This study investigated four different prototypes of the innovative

**Table 2**  
Mechanical properties of all the main parts of the system.

Material	Density (g/cc)	Tensile strength	Tensile strength (Yield) (MPa)	Elongation at break (%)	Tensile modulus (GPa)	Poisson's ratio
AL6063	2.70	150	90	20	69	0.33
AL6061	2.70	310	276	12–17	68.9	0.33
SUS304	8.00	590	330	40	193	0.29
SS400	7.80	415	205	21	160	0.25

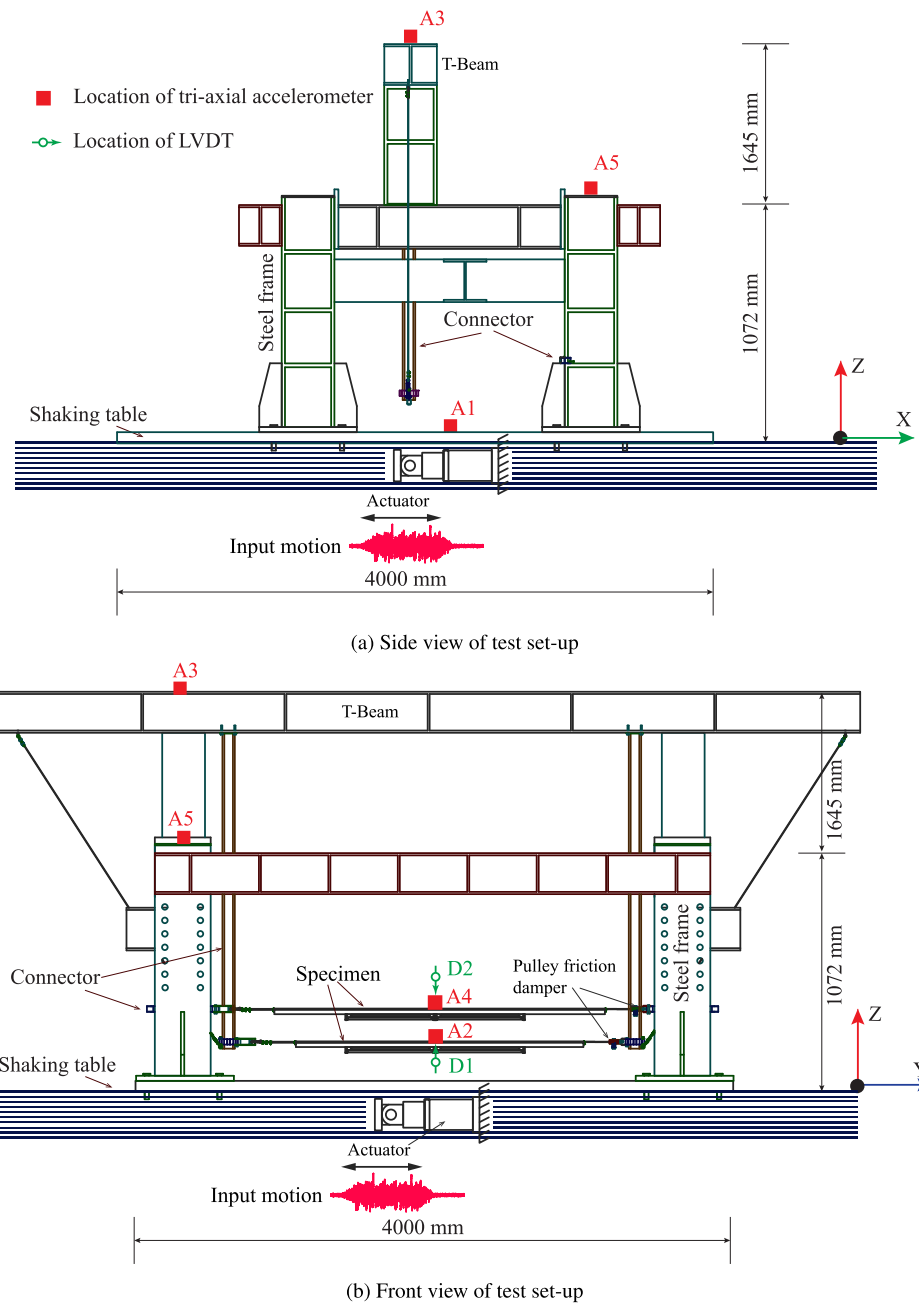


Fig. 3. Shaking table test set-up.

wireway vibration attenuation system, each of which utilized a different connector type: Ceiling (CT), H-beam frame (HBT), Wall (WT), and Beam-column (BCT). The specimens were given names based on the connector and the main component they were attached. Details of the four specimens are depicted in Fig. 1.

A friction damper with a 60mm diameter pulley was installed for each prototype, as shown in Fig. 2. The damper can dissipate seismic energy via mechanical friction between the pulley and the pulley base, the cable and the pulley, as well as friction between the pulley and the aluminum pipe [44].

All specimens were fabricated with the same length of 3680 mm. In each specimen, a 34W LED with a 1070 mm length was mounted on a  $65 \times 70 \times 2500$  mm aluminum duct. Two parallel cables connected to a tension towing machine were used to suspend the luminaire unit that included a duct and a LED light. The pre-tension at both ends of the cable was 1500N. The compression force of the spring was 120N. Each

specimen weighs approximately 27 kg. The four specimens can be classified into two groups: “pole connector” (CT and BCT) and “direct connector” (WT and HBT). Note that, for each pole connector specimen, two cable bracing systems are used to connect the two poles to the main structure to avoid pole failure from lateral loads, and to strengthen the stability of the system under seismic loads. The pole lengths of the CT and BCT specimens were 2150 mm and 760 mm, respectively.

Aluminized alloy grade AL6063 was used to fabricate the poles and the duct. The pulley was made of AL6061 grade aluminized alloys. The cable was composed of stainless steel and had a diameter of 4mm. All of the bolts and anchor bolts were manufactured of SS400 steel. The end base and pulley base were all made of SUS304 grade steel. The mechanical characteristics of the cable are shown in Table 1. The material properties of the stainless steel and aluminum alloy used for the rest of the parts are provided in Table 2.

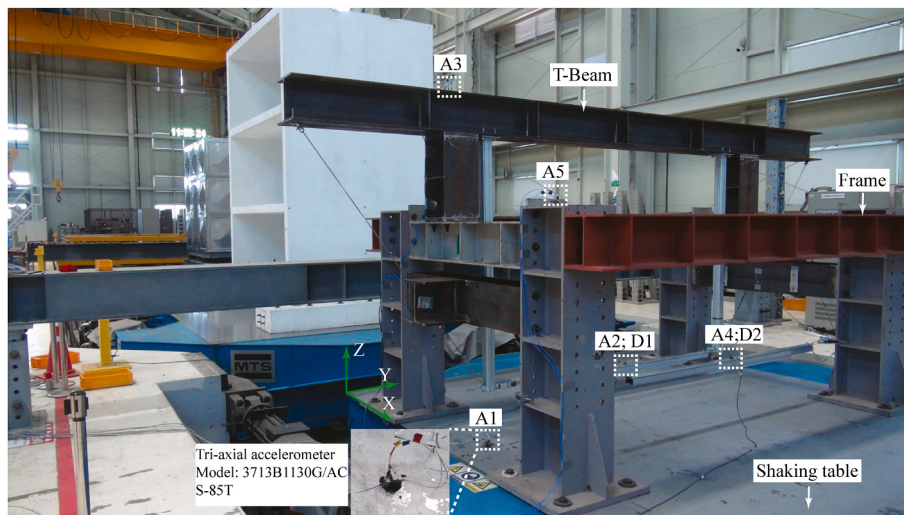


**Fig. 4.** The locations of the accelerometers and LVDTs from phase Test I.

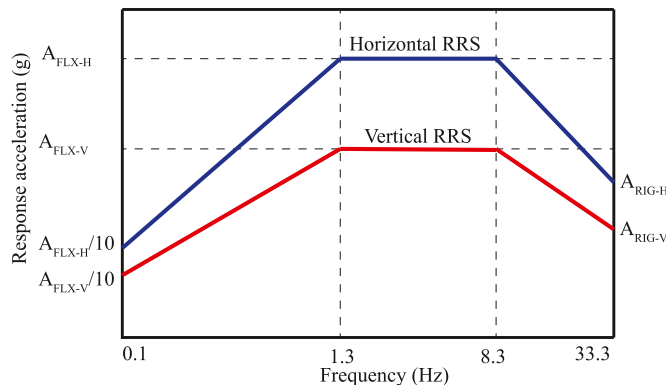


**Fig. 5.** Required response spectrum (AC156).

**Table 3**  
Test plan and test protocol.

Test phase	Test No.	Specimen under test	S <sub>DS</sub> (g)
I	1	Ceiling and H-beam frame	1.00
	2		1.00
	3		1.00
II	1	Wall	1.00
III	1	Beam-column	1.00
	2		1.00

## 2.2. Test setup and measuring instruments

The shaking table test was carried out at the Seismic Research And Test Center of Pusan National University. The details of the shaking table test setup for the four specimens are provided in Fig. 3. The shaking table was an electro-hydraulic servo with three variable controls, and six degrees of freedom (X, Y, Z, RX, RY, RZ). The table measures 4 × 4 meters in size, with a payload capacity of 30 000 kg.

In this study, a two-story, one-bay steel stiff frame, capable of transmitting seismic input to the test specimen, was specially designed and fabricated for conducting dynamic tests using an isolated shaking table. It was used to replicate the structure of a single room within the building where the systems would be mounted. The first floor of the steel frame was made up of four steel beams and four steel columns. The second level of the steel frame was composed of a single steel T-beam

and two steel columns that were bolted to the steel beam of the first floor.

To record the acceleration and displacement responses of the specimens and steel frame in three orthogonal directions during the tests, a total of five tri-axial accelerometers and two static linear variable displacement transducers (LVDTs) were employed. Four specimens were tested in three separate phases, which were referred to as Test I (CT and HBT specimens), Test II (WT specimen), and Test III (BCT specimen). Accelerometer A1 was placed at the base of the shaking table. Accelerometers A3 and A5 were installed at the top of the T-beam and the top of the steel column on the first floor, respectively. The acceleration and the displacement responses recorded by accelerometers A2 and A4, LVDT D1 and D2 at the top midpoint of the duct, were used to evaluate and compare the earthquake performances of the specimens. The actual image of the locations of accelerometers and LVDTs from phase Test I is depicted in Fig. 4.

## 2.3. Input ground acceleration records

Shake table tests were conducted according to the loading protocol recommended by ICC-ES-AC 156 [45], which has been widely used to evaluate the seismic performance of NSCs. The used seismic input was generated to satisfy the required response spectrum (RRS), which is the lowest seismic acceleration required to excite a target component as a function of the natural period or natural frequency. The RRS developed from the two parameters: the story height ratio ( $z/h$ ), and the design spectral response acceleration at short periods  $S_{DS}$  [46–48]. The seismic parameters including the horizontal and vertical spectral acceleration for flexible and rigid components were used to calculate the RRS levels, as shown in Fig. 5.

The horizontal spectral acceleration for flexible  $A_{FLX-H}$  and rigid  $A_{RIG-H}$  components are computed as follows [45,49]:

$$A_{FLX-H} = S_{DS} \left( 1 + 2 \frac{z}{h} \right) \leq 1.6 S_{DS} \quad (1)$$

$$A_{RIG-H} = 0.4 S_{DS} \left( 1 + 2 \frac{z}{h} \right) \quad (2)$$

The vertical spectral acceleration of the flexible  $A_{FLX-V}$  and rigid  $A_{RIG-V}$  components are computed as follows [45,49]:

$$A_{FLX-V} = 0.67 S_{DS} \quad (3)$$

$$A_{RIG-V} = 0.27 S_{DS} \quad (4)$$

An artificial acceleration record corresponding to  $S_{DS} = 1.0$  g was

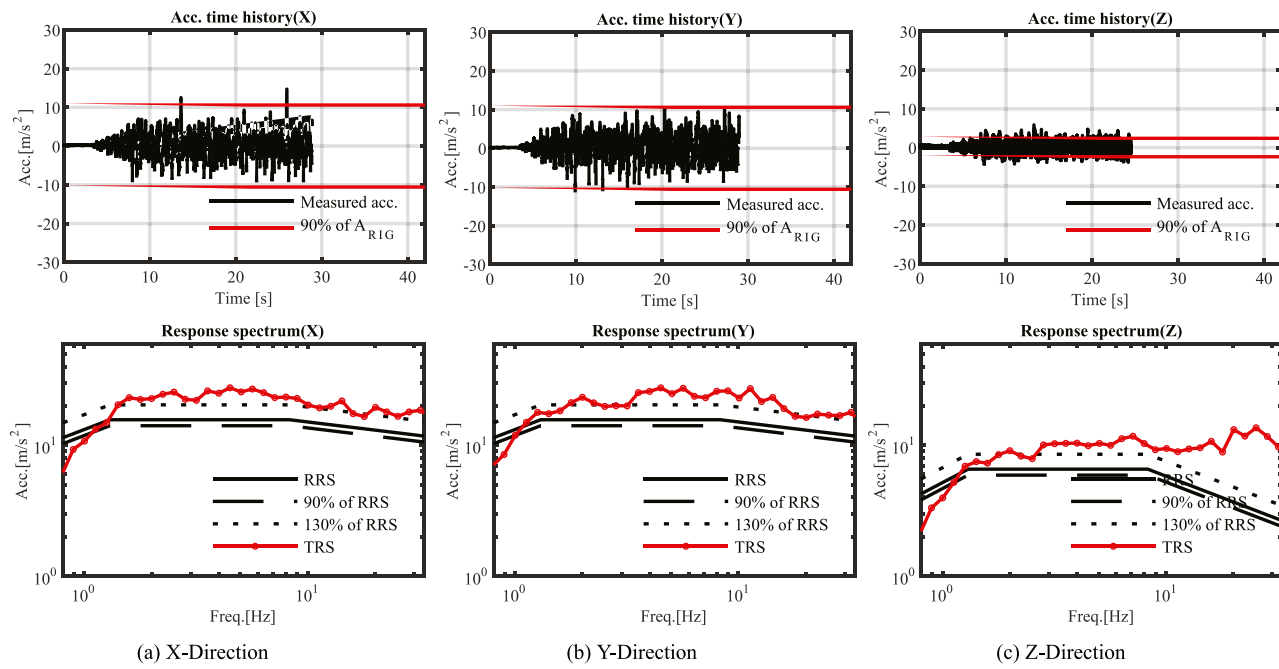


**Fig. 6.** Input acceleration time history corresponding to  $S_{DS} = 1.0$  g, TRS, RRS, upper and lower matching limits.

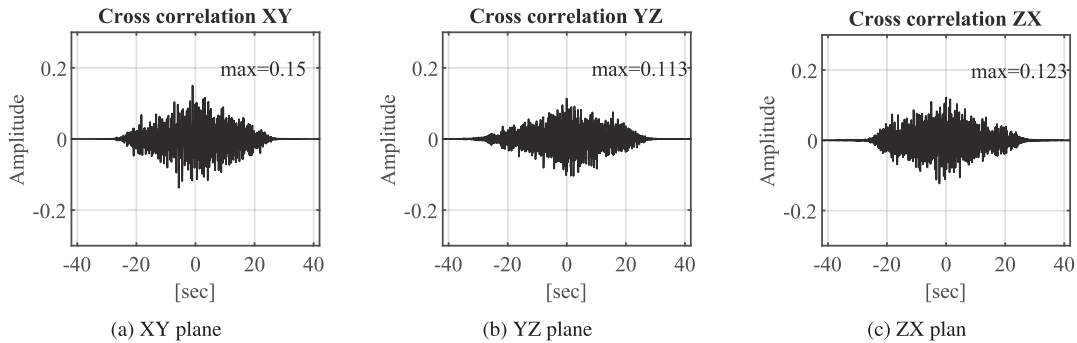


**Fig. 7.** Correlation coefficient of the input motion.

applied to test specimens. A test plan is summarized in Table 3.

This study assumed that the specimens were attached to the top floor of the structures, making it reasonable to set  $z/h = 1.0$ . Figure 6 shows the input acceleration time-history, its elastic response spectrum for damping value of 5%, namely the test response spectrum (TRS), the RRS, and the RRS scaled to 90 and 130%. This input acceleration time-history was generated by engineers of the Seismic Research And Test Center of Pusan National University. The figure clear shows that the input acceleration met the ICC-ES AC156 and SPS-F KOCEP 0007-7419:2021 requirements [45,49]. Fig. 7 shows the correlation coefficients of the input acceleration time-history. The maximum cross-correlation function coefficients for the XY, YZ, and ZX planes were 0.15, 0.113, and 0.123, respectively. These values are all less than 0.3, satisfying the IEEE Std. 344 criteria for the statistical independence of ground motions [50].

### 3. Test results and discussion

#### 3.1. Fundamental frequency of the specimens

Before the shaking table test, the resonance frequency search tests were conducted to determine the fundamental frequencies and dynamic characteristics of the specimens. Following FEMA 461 [51], these tests were conducted with single-axis sinusoidal sweeps at the rate of two

octaves/min. Tests were performed consecutively within the frequency range of 1.0–50 Hz, corresponding to each orthogonal major axis. The fundamental frequencies of the specimens were calculated using the frequency domain transfer function technique [52]. The raw experimental data was evaluated using a program written in MATLAB version R2020a [53]. Fig. 8 illustrates the transfer function charts for Test I, Test II, and Test III.

The fundamental frequency results for the four different specimens and the steel frame are shown in Table 4. The results show that the fundamental frequencies were between 8 and 19.75 Hz. For the steel frame, the fundamental frequencies in the X and Y directions obtained in all tests were essentially identical for accelerometers A3 and A5. These investigations were unable to estimate a fundamental frequency in the Z direction. Therefore, it was determined that the frame was sufficiently rigid to avoid unintentional amplification of the table input motion in the test frame.

The fundamental frequency values for the specimens varied depending on the method of connection to the main structure. The WT specimen was determined to be the stiffest in the X (14.00 Hz) and Z (9.25 Hz) directions, while the CT and HBT specimens were the stiffer in the Y directions (19.75 Hz). In comparison, the stiffness of the CT and BCT specimens were lowest in the X (11.75 Hz) and Z (8.00 Hz) directions, respectively, while the stiffness of the HBT specimen was

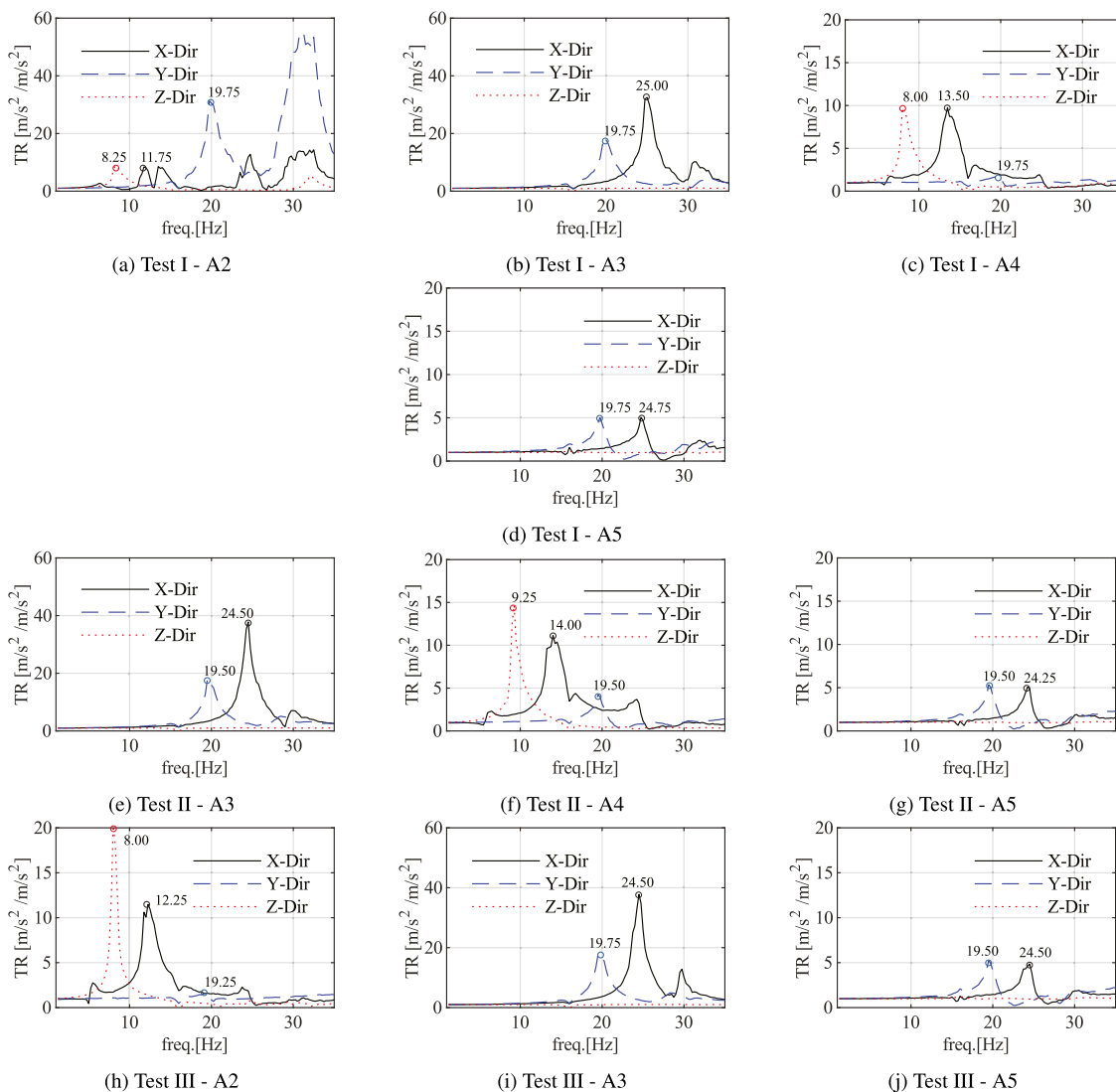


Fig. 8. The transfer function plot of the phase Test I, Test II and Test III.

**Table 4**  
The fundamental frequency results.

Test phase	Specimen	Location	Fundamental frequency (Hz)			Remark
			X-Dir	Y-Dir	Z-Dir	
Test I	Ceiling	A2	11.75	19.75	8.25	Fig. 8a
	Top of the T-beam	A3	25.00	19.75	N/A	Fig. 8b
	H-beam	A4	13.50	19.75	8.00	Fig. 8c
	Top of the column	A5	24.75	19.75	N/A	Fig. 8d
Test II	Top of the T-beam	A3	24.50	19.50	N/A	Fig. 8e
	Wall	A4	14.00	19.50	9.25	Fig. 8f
	Top of the column	A5	24.25	19.50	N/A	Fig. 8g
Test III	Beam-column	A2	12.25	19.25	8.00	Fig. 8h
	Top of the T-beam	A3	24.50	19.75	N/A	Fig. 8i
	Top of the column	A5	24.25	19.50	N/A	Fig. 8j

lowest in the Y direction (19.25 Hz). The specimen with the longer poles was the CT specimen (11.75 Hz), which was less stiff in the X dimension than the BCT specimen (12.25 Hz). In comparison, the stiffness of the CT specimen was greater than that of the BCT specimen in the Y and Z directions.

### 3.2. Visual inspection

Prior to and following testing, the four specimens were visually inspected for deformation and damage. After visual inspection, a series of shaking table tests found no significant structural failure in the four specimens and no significant damage at the bolt connections and connectors. None of the specimens toppled over or collapsed, and the lights continued to work smoothly. Therefore, the results confirmed that the innovative wireway vibration attenuation system specimens would operate efficiently during an earthquake satisfying the ICC-ES AC156 and SPS-F KOCED 0007-7419:2021 standards [45,49].

### 3.3. Evaluating the effect of connectors on seismic performance

The lateral displacement (X direction) response-time histories at the center of the four specimens were recorded using LVDT D1 and D2. The

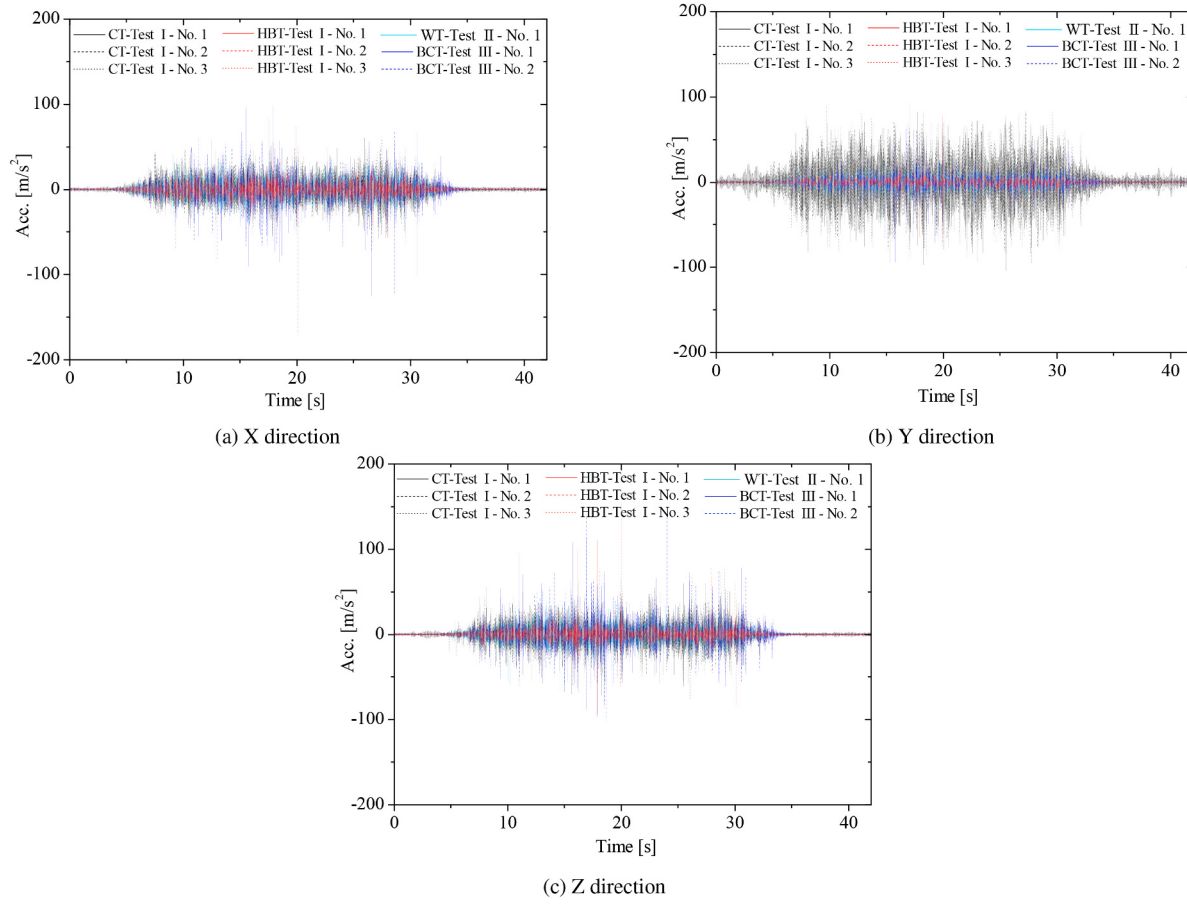


**Fig. 9.** The response acceleration time history plots of the four specimens.

results show that there was no discernible change in the displacements of the four test specimens. Therefore, the connectors have no noticeable impact on the system's response displacement.

### 3.3.2. Acceleration response

Fig. 9a–c shows the acceleration response results measured at the center of the specimens in the X, Y, and Z directions. Black, red, cyan, and blue represent the acceleration responses of the CT, HBT, WT, and BCT specimens, respectively.

To determine the effect of the connectors on the acceleration response of the systems, the graph superposition approach was utilized. On the same graph, the acceleration responses of the four specimens were plotted in the time domain. As the plot area increases, the acceleration response increases. As can be observed, the red area was the smallest in three directions X, Y, and Z, indicating that the HBT specimen had the lowest acceleration response. In comparison, the areas of black and blue were the greatest in the X and Z directions, showing that the acceleration responses of the BCT and CT specimens were the largest. Notably, the acceleration response in the Y direction of the CT specimen was extremely high, compared to the others. This proves that connectors with large pole lengths are not recommended in this system.

### 3.3.3. Peak resonant oscillation

The behavior of the specimens needs to be carefully considered when resonance occurs during earthquakes. Therefore, a comprehensive and detailed investigation of the frequency domain was performed. The acceleration spectral density (ASD) [54] depicts the acceleration response distribution for each frequency measured using the shaking table experiment. An approach for calculating the ASD functions of the measured data is Welch's method [55,56]. Denote the  $m$ th windowed,

zero-padded frame from the signal  $x$  as follows:

$$x_m(n) \triangleq \omega(n)x(n + mR) \quad (5)$$

$n = 0, 1, \dots, M - 1, m = 0, 1, \dots, K - 1$  where  $R$  is defined as the window hop size and let  $K$  denote the number of available frames. Then, the periodogram of the  $m$ th block is given by:

$$P_{x_m, M}(\omega_k) = \frac{1}{M} |\text{FFT}_{N, k}(x_m)|^2 \triangleq \frac{1}{M} \left| \sum_{n=0}^{N-1} x_m(n) e^{-j2\pi nk/N} \right|^2 \quad (6)$$

the Welch estimate of the power spectral density is as follows:

$$\hat{S}_x^w(\omega_k) \triangleq \frac{1}{K} \sum_{m=0}^{K-1} P_{x_m, M}(\omega_k) \quad (7)$$

Fig. 10a–c depicts ASD plots of the four different specimens in the X, Y, and Z directions, respectively. Acceleration spectra were calculated using the Welch function in MATLAB [53]. The ASD values between 1 and 256 Hz are displayed. The following parameters were used to calculate ASD in this study:  $M = 1024$  points per segment,  $K = 21$ , segments with 50% duplicates  $S = 0.5$  M, time per segment = 2 s, and  $df = 0.5$  Hz were utilized as the input parameters for the ASD calculation.

The peak ASD values when resonance occurred and the corresponding frequencies of the four specimens are shown in Table 5. The specimens with the pole connectors (CT and BCT) show higher peak resonant oscillations than those with the direct connectors (WT and HBT). An ASD mean value for a specimen is the average of the ASD values from all the tests performed on the specimen. The HBT specimen has the smallest peak ASD mean values of  $0.0384 \text{ G}^2/\text{Hz}$ ,  $0.0018 \text{ G}^2/\text{Hz}$ ,

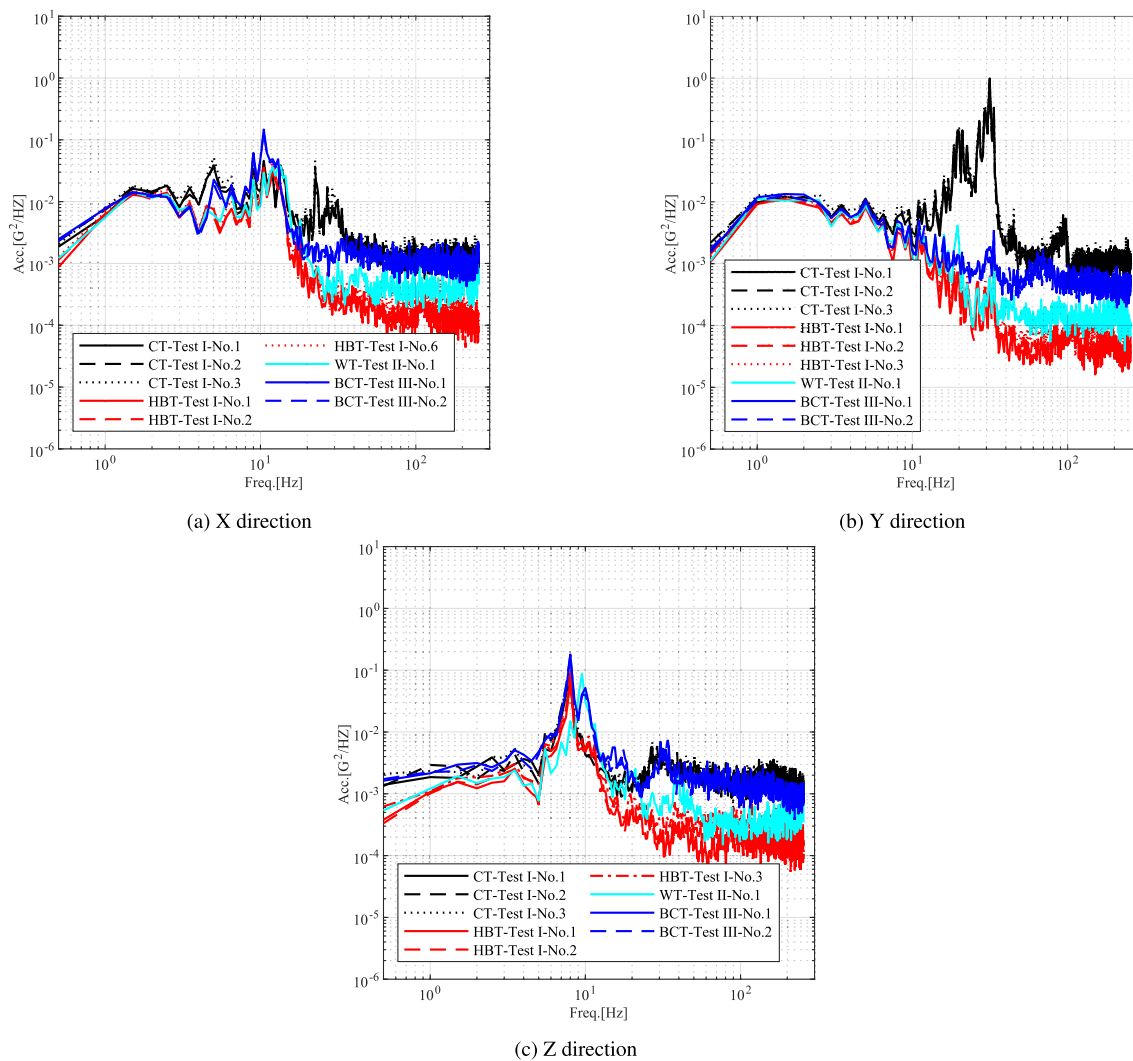


Fig. 10. ASD plots of the four specimens.

**Table 5**  
The maximum ASD value and corresponding frequency the specimens.

Test phase	Test no.	Specimen under test	z (m)	$S_{DS}$ (g)	Middle position					
					X-Dir		Y-Dir		Z-Dir	
					ASD ( $G^2/Hz$ )	Freq. (Hz)	ASD ( $G^2/Hz$ )	Freq. (Hz)	ASD ( $G^2/Hz$ )	Freq. (Hz)
Test I	1	Ceiling	2.430	1.00	0.0458	10.50	0.9941	31.50	0.0629	8.00
		H-beam frame	0.505	1.00	0.0318	12.00	0.0017	33.50	0.0662	8.00
	2	Ceiling type	2.430	1.00	0.0349	10.50	0.8642	31.50	0.0809	8.00
		H-beam frame	0.505	1.00	0.0370	12.00	0.0018	33.50	0.0821	8.00
	3	Ceiling	2.430	1.00	0.0414	10.50	0.9414	31.50	0.1290	8.00
		H-beam frame	0.505	1.00	0.0463	12.00	0.0018	33.50	0.1012	8.00
Test II	1	Wall	1.070	1.00	0.0373	13.50	0.0112	19.50	0.0872	9.50
Test III	1	Beam-column	1.070	1.00	0.1471	10.50	0.0033	33.50	0.1799	8.00
	2	Beam-column	1.070	1.00	0.1299	10.50	0.0035	33.50	0.1782	8.00

and  $0.0832 G^2/Hz$  in the X, Y, and Z directions, respectively, indicating that it had the lowest peak oscillations when resonance occurred. In comparison, the BCT specimen showed the largest peak ASD mean values in the X and Z directions when resonance occurred, at  $0.1385 G^2/Hz$  and  $0.1791 G^2/Hz$ . Notably, the peak ASD mean value in the Y direction of the CT specimen was extremely large compared to the other specimens, about  $0.9332 G^2/Hz$ , almost 518.44, 83.32 and 274.47 times

that of the HBT, WT and BCT specimens. This proves that connectors with large pole lengths are not recommended in this system.

### 3.3.4. Earthquake energy dissipation

The root mean square acceleration (GRMS) [57] is a measure of the energy accumulated in a structure as a result of an earthquake. In the frequency domain, the GRMS is defined as the square root of the area

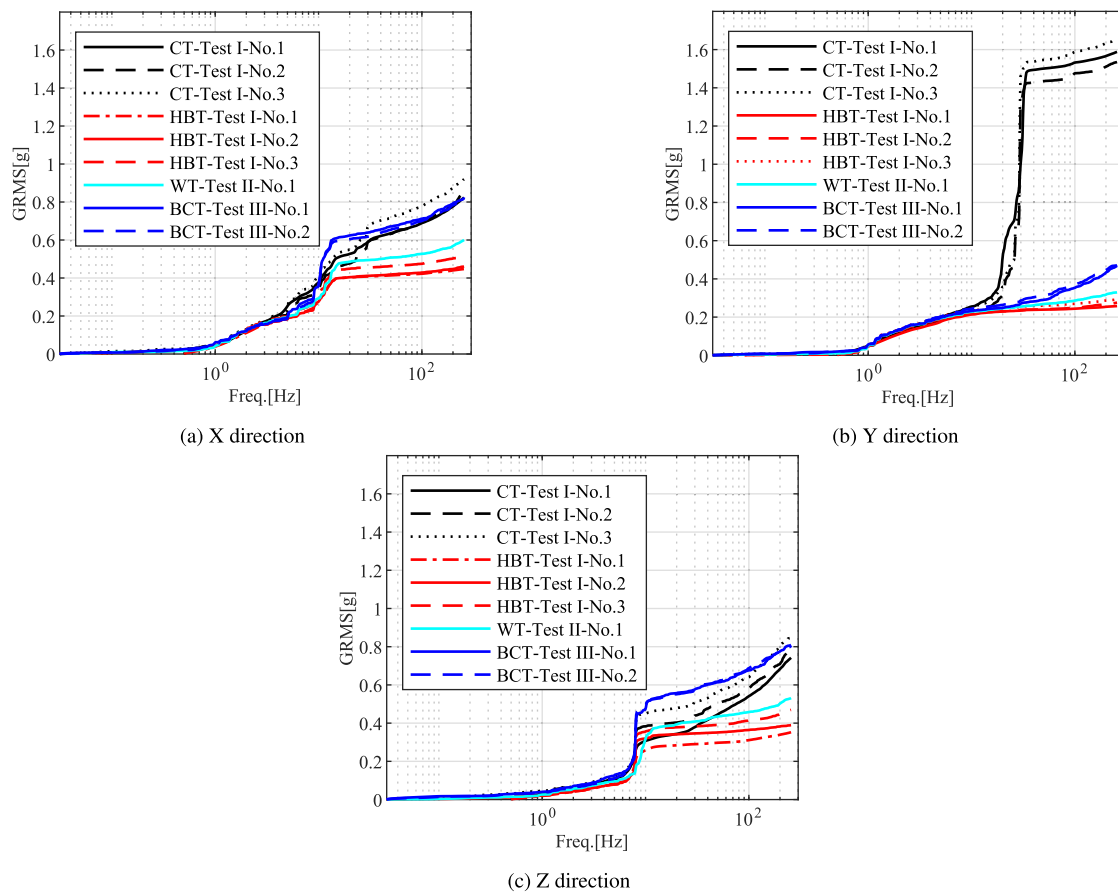


Fig. 11. Cumulative acceleration root mean square plots of the four specimens.

**Table 6**  
Overall GRMS value of the specimens.

Test phase	Test no.	Specimen under test	$z$ (m)	$S_{DS}$ (g)	Overall GRMS			Pole length (mm)
					Middle position			
					X-Dir	Y-Dir	Z-Dir	
Test I	1	Ceiling	2.430	1.00	0.8234	1.588	0.7421	2150
		H-beam frame	0.505	1.00	0.4471	0.2579	0.3527	
	2	Ceiling	2.430	1.00	0.8479	1.535	0.7773	
		H-beam frame	0.505	1.00	0.4607	0.2756	0.3894	
	3	Ceiling	2.430	1.00	0.9196	1.652	0.8491	2150
		H-beam frame	0.505	1.00	0.5147	0.2923	0.4693	
Test II	1	Wall type	1.070	1.00	0.6001	0.3296	0.5313	760
Test III	1	Beam-column	1.070	1.00	0.8246	0.4681	0.8095	
	2	Beam-column	1.070	1.00	0.8222	0.4724	0.8053	

**Table 7**  
Overall GRMS of acceleration response of the frame.

Test phase	Test no.	$S_{DS}$ (g)	A1 ( $z = 0$ m)			A5 ( $z = 1.645$ m)			A3 ( $z = 2.717$ m)		
			X-Dir	Y-Dir	Z-Dir	X-Dir	Y-Dir	Z-Dir	X-Dir	Y-Dir	Z-Dir
Test I	1	1.00	0.244	0.251	0.112	0.271	0.280	0.129	0.560	0.457	0.132
	2	1.00	0.244	0.251	0.112	0.259	0.286	0.119	0.527	0.465	0.112
	3	1.00	0.244	0.251	0.112	0.280	0.298	0.126	0.573	0.489	0.119
Test II	1	1.00	0.244	0.251	0.112	0.266	0.295	0.118	0.582	0.479	0.110
Test III	1	1.00	0.244	0.251	0.112	0.268	0.294	0.132	0.584	0.480	0.113
	2	1.00	0.244	0.251	0.112	0.267	0.296	0.118	0.579	0.482	0.109

**Table 8**

Overall GRMS of the frame based on the mounting position of the specimen.

Test phase	Test no.	Specimen under test	$z$ (m)	$S_{DS}$ (g)	Overall GRMS (g)		
					Mounting position		
					X-Dir	Y-Dir	Z-Dir
Test I	1	Ceiling H-beam frame	2.430	1.00	0.4826	0.4096	0.1312
		Ceiling H-beam frame	0.505	1.00	0.2537	0.2495	0.1463
	2	Ceiling H-beam frame	2.430	1.00	0.4553	0.4171	0.1139
		Ceiling H-beam frame	0.505	1.00	0.2438	0.2562	0.1155
Test II	1	Wall	1.070	1.00	0.2583	0.2796	0.1159
	1	Beam-column	1.070	1.00	0.2607	0.2814	0.1341
Test III	2	Beam-column	1.070	1.00	0.2593	0.2806	0.1152

under the ASD curve. The area under the ASD curve of the  $j$ th frequency segment ( $a_j$ ) between the frequencies  $f_{i-1}$  and  $f_i$  corresponds to  $P_{i-1}$  and  $P_i$  [58].

$m$  is the slope of the segment  $j$  between the frequencies  $f_{i-1}$  and  $f_i$ :

$$m = 10 \log\left(\frac{P_i}{P_{i-1}}\right) \frac{\log(2)}{\log\left(\frac{f_i}{f_{i-1}}\right)} \quad (8)$$

for  $m \neq -10 \log(2)$ :

$$a_{f_i,j} = 10 \log(2) \frac{P_i}{10 \log(2) + m} \left[ f_i - f_{i-1} \left( \frac{f_{i-1}}{f_i} \right)^{m/10 \log(2)} \right] \quad (9)$$

for  $m = -10 \log(2)$ :

$$a_{f_i,j} = P_{i-1} f_{i-1} \ln\left(\frac{f_i}{f_{i-1}}\right) \quad (10)$$

The GRMS value at the  $j$ th frequency segment:

$$\text{GRMS}_j = \sqrt{a_j} \quad (11)$$

The overall GRMS level at  $j$ th at frequency  $f_i$  is then:

$$\text{GRMS}_{f_i} = \sum_{m=0}^j a_m \quad (12)$$

The cumulative GRMS curves (CRMS) depicted in Fig. 11a–c correspond to the X, Y, and Z directions. The CRMS for the four specimens is divided into 3 ranges: low frequency (0–8 Hz), resonance (8–31.5 Hz), and high frequency (>31.5 Hz). In the low frequency range, the CRMS of the four specimens were substantially identical. The differences in seismic energy between the specimens occurred primarily in the resonant and high frequency ranges.

The overall GRMS is the value at the end of the CRMS, as shown in Table 6. According to this indicator, the HBT specimen had the lowest earthquake energy during the test, with overall GRMS mean values of 0.4742 g, 0.2753 g, and 0.4038 g in the X, Y, and Z directions. The CT specimen had the highest seismic energy in the X, and Y directions, with overall GRMS mean values of 0.8636 g, 1.5917 g. The BCT specimen had the highest seismic energy in the Z directions, with overall GRMS mean values of 0.8074 g. Notably, with a pole length of 2150mm, the CT specimen had earthquake energy about 5.78, 4.83, and 3.38 times greater than the HBT, WT and BCT specimens in the Y direction. This proves that connectors with large pole lengths are not recommended in this system.

The overall GRMS of acceleration response at the base of the shaking test table, the top of the T-beam, and the top of the column of the frame in Test I, Test II and Test III are shown in Table 7. From this result, the overall GRMS of the frame at the mounting position of each specimen

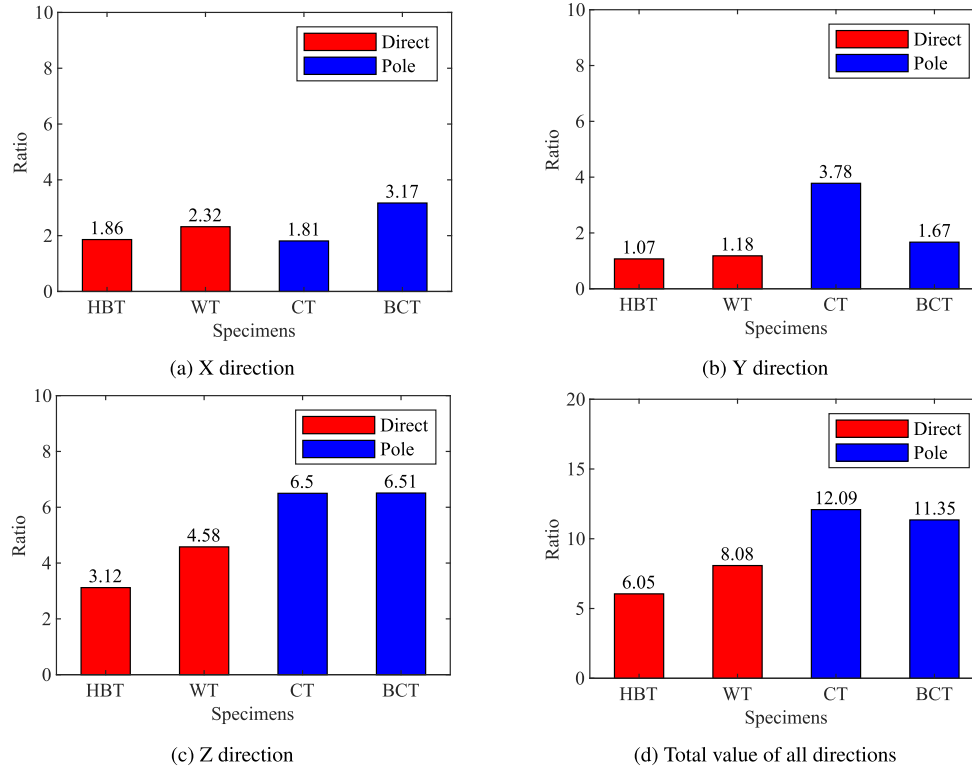


Fig. 12. Energy transmission ratio plots of the four specimens.

was derived using the interpolation approach, based on the mounting height of the specimen in the steel frame, as indicated in Table 8. It is clear that the overall GRMS value grows as the height on the frame is increased. Because the specimens were suspended at varying heights on the frame, an “energy transmission ratio” (ETR) is proposed to precisely assess the influence of connectors on the seismic energy generated by the system without considering the installation height. This is the ratio of the overall GRMS of each specimen to the overall GRMS of the frame at its suspension location. The specimen with a smaller ETR coefficient is more effective at dissipating seismic energy.

The ETR coefficients for the two types of connectors are depicted in Fig. 12. Red indicates the ETR values of specimen with the direct connectors (WT and HBT), whereas the blue indicates the ETR values of specimen with the pole connectors (CT and BCT). The ETR values depicted in this figure are the average of the ETR values obtained from all tests in which the specimen was tested.

Based on the total ETR values of all directions, it is clear that the specimens with the direct connectors (HBT and WT) had excellent seismic performance, 1.4–2.0 times higher than the specimens with the pole connectors (CT and BCT). The HBT was the most effective at dissipating earthquake energy, with the lowest total ETR coefficients in all directions of 6.05. The CT specimen had the highest total ETR coefficient of 12.09 in three directions, about 2.00 and 1.50 times greater than HBT and WT specimens, indicating that it was the lowest energy-dissipating capacity system. As a result, direct connectors are proposed for this novel system in order to minimize the risk of system failure during an earthquake.

It was determined that the length of the pole has an influence on the system's energy dissipation in both the X and Y directions, but has no effect on its energy dissipation in the Z direction. The CT specimen has an ETR coefficient that is 1.75 times smaller than that of BCT specimen in the X direction. In comparison, the ETR coefficient of CT specimen is 2.263 times greater than that of BCT specimen in the Y direction. In the Z direction, the ETR coefficients of the two specimens are nearly identical, at approximately 6.5.

Based on the findings of this experimental study, for the raceway LED light fixtures with pole connectors, the authors recommend that if the pole lengths exceed 1500 mm, designers should reinforce the connections of the systems in the Y and Z directions. Otherwise, the connections in the X and Z directions should be reinforced. For the systems with the direct connectors, the authors recommend strengthening the system's connections in the X and Z directions.

It is clear that the seismic energy in the Z direction accounted for the greatest proportion of the total seismic energy of the four specimens, ranging from 51.57% to 57.36%. As a result, additional seismic energy dissipation mechanisms in the Z direction are required for this novel system, which will be considered in the further study.

#### 4. Conclusion

This study evaluated the seismic performance of an innovative wireway vibration attenuation system with several typical connectors, for exposed raceway light fixtures using tri-axial shaking table tests. To address this, four prototypes were fabricated with connectors suitable for mounting on a variety of structural components, including the ceiling (CT), H-beam frame (HBT), wall (WT), and beam and column (BCT). The input motion for the tri-axial shaking table tests was generated according to the ICC-ES AC156 standard. The following primary conclusions can be drawn from the test findings.

- A series of tri-axial shaking table tests that satisfied the AC156 standard were conducted, and proved that the system would perform efficiently during an earthquake.
- The initial natural frequencies of the specimens in the X, Y, and Z directions were determined to be between 8 and 19.75 Hz.

- The connector had no discernible effect on the response displacement of the system.
- The specimens with the pole connectors (CT and BCT) show higher peak resonant oscillations than those with the direct connectors (WT and HBT). The peak resonant oscillation in the Y direction of the CT specimen was extremely large compared to the other specimens. It proves that connectors with large pole lengths are not recommended in this system.
- The HBT and CT specimens had the lowest and highest earthquake energy, respectively. Differences in the seismic energy of the specimens occurred primarily in the resonant and high frequency ranges. The CT specimen had earthquake energy about 3.38–5.78 times greater than the other specimens in the Y direction. This proves that connectors with large pole lengths are not recommended in this system.
- The specimens with the direct connectors had excellent seismic performance, 1.4–2.0 times higher than those with the pole connectors. As a result, direct connectors are proposed for this novel system in order to minimize the risk of system failure during an earthquake. Furthermore, the length of the poles has an influence on system's energy dissipation in both the X and Y directions, but has no effect on its energy dissipation in the Z direction.
- The additional seismic energy dissipation mechanisms in the Z direction are required for the innovative wireway vibration attenuation system, which will be considered in a further study.

This study developed an innovative wireway vibration attenuation system with friction damper to increase the survivability of exposed raceway light fixtures during an earthquake. The seismic performance of the specimens connected to the wall, beam, column, steel H-beam frame, and ceiling components were studied. The experimental testing is planned to evaluate the seismic performance of full-scale specimens with a length of 25 meters which will be presented in the following research.

#### Declaration of Competing Interest

The authors declare the following financial interests/personal relationships which may be considered as potential competing interests.

#### Data availability

The authors do not have permission to share data.

#### Acknowledgements

This research is the projects funded by Sehong Inc. Ltd in 2020. This work was supported by Ministry of Land, Infrastructure and Transport of Korean Government (22TBIP-C161540-02).

#### References

- [1] R. Villaverde, Seismic design of secondary structures: state of the art, *J. Struct. Eng.* 123 (8) (1997) 1011–1019.
- [2] E. FEMA, Reducing the Risks of Nonstructural Earthquake Damage, Practical Guide, January, 2010.
- [3] C.A. Kircher, It Makes Dollars and Sense to Improve Nonstructural System Performance, *PROC ATC 29-2 Seminar On Seismic Design, Performance and Retrofit OF*, 2003.
- [4] A. Filiatrault, T. Sullivan, Performance-based seismic design of nonstructural building components: the next frontier of earthquake engineering, *Earthquake Eng. Vibrat.* 13 (1) (2014) 17–46.
- [5] D. Ding, C. Arnold, H. Lagorio, S. Tobriner, S. Rihal, R. Mangum, G. Hezmalhalch, M. Green, A. Watson, D. Mah, et al., Architecture building contents, and building systems, *Eathquake Spectr.* 6 (S1) (1990) 339–377.
- [6] L. Qi, M. Kurata, Y. Ikeda, K. Kunimoto, M. Takaoka, Seismic evaluation of two-elevation ceiling system by shake table tests, *Earthquake Eng. Struct. Dyn.* 50 (4) (2021) 1147–1166.
- [7] K.A. Institute, Pohang Earthquake Damage Survey Report, Korea Architectural Institute, Seoul, Korea, 2018.

- [8] G. Magliulo, M. Ercolino, C. Petrone, O. Coppola, G. Manfredi, The emilia earthquake: seismic performance of precast reinforced concrete buildings, *Eathquake Spect.* 30 (2) (2014) 891–912.
- [9] E. Miranda, G. Mosqueda, R. Retamales, G. Pekcan, Performance of nonstructural components during the 27 february 2010 chile earthquake, *Eathquake Spect.* 28 (1\_suppl1) (2012) 453–471.
- [10] R.P. Dhakal, G.A. MacRae, K. Hogg, Performance of Ceilings in the February Christchurch Earthquake, 2011.
- [11] K. Kasai, A. Mita, H. Kitamura, K. Matsuda, T.A. Morgan, A.W. Taylor, Performance of seismic protection technologies during the 2011 tohoku-oki earthquake, *Eathquake Spect.* 29 (1\_suppl) (2013) 265–293.
- [12] D. Wang, J. Dai, Z. Qu, X. Ning, Shake table tests of suspended ceilings to simulate the observed damage in the m s 7.0 lushan earthquake, China, *Earthquake Eng. Eng. Vibrat.* 15 (2) (2016) 239–249.
- [13] J. Iyama, S. Matsuo, S. Kishiki, T. Ishida, K. Azuma, M. Kido, T. Iwashita, K. Sawada, S. Yamada, T. Seike, Outline of reconnaissance of damaged steel school buildings due to the 2016 Kumamoto earthquake, *AIJ J. Technol. Design* 24 (56) (2018) 183–188.
- [14] D. Perrone, P. Calvi, R. Nascimbene, E. Fischer, G. Magliulo, Seismic performance of non-structural elements during the 2016 central Italy earthquake, *Bull. Earthquake Eng.* 17 (10) (2019) 5655–5677.
- [15] H. Badillo-Almaraz, A.S. Whittaker, A.M. Reinhorn, Seismic fragility of suspended ceiling systems, *Eathquake Spect.* 23 (1) (2007) 21–40.
- [16] J. McCormick, Y. Matsuoka, P. Pan, M. Nakashima, Evaluation of non-structural partition walls and suspended ceiling systems through a shake table study, in: *Structures Congress, Crossing Borders*, 2008, pp. 1–10.
- [17] Y. Matsuoka, K. Saita, S. Yamada, Y. Shimada, M. Akazawa, Non-structural component performance in 4-story frame tested to collapse, in: *Proceedings of the 14th World Conference on Earthquake Engineering*, 2008, pp. 12–17.
- [18] R. Retamales, G. Mosqueda, A. Filiatrault, A. Reinhorn, Testing protocol for experimental seismic qualification of distributed nonstructural systems, *Eathquake Spect.* 27 (3) (2011) 835–856.
- [19] G. Magliulo, V. Pantagelo, G. Maddaloni, V. Capozzi, C. Petrone, P. Lopez, R. Talamonti, G. Manfredi, Shake table tests for seismic assessment of suspended continuous ceilings, *Bull. Earthquake Eng.* 10 (6) (2012) 1819–1832.
- [20] A.S. Gilani, S.M. Takhirov, L. Tedesco, Seismic evaluation procedure for suspended ceilings and components, new experimental approach, in: *Proceedings of the 15th World Conference on Earthquake Engineering*, 2012.
- [21] K. Ryu, A. Reinhorn, A. Filiatrault, Full scale dynamic testing of large area suspended ceiling system, in: *Proceedings of the 15th World Conference on Earthquake Engineering*, Lisbon, Portugal: WCEE 5474, 2012.
- [22] E. Pantoli, M.C. Chen, X. Wang, R. Astroza, H. Ebrahimi, T.C. Hutchinson, J. P. Conte, J.I. Restrepo, C. Marin, K.D. Walsh, et al., Full-scale structural and nonstructural building system performance during earthquakes: part II-NCS damage states, *Eathquake Spect.* 32 (2) (2016) 771–794.
- [23] S.-C. Jun, C.-H. Lee, C.-J. Bae, K.-J. Lee, Shake-table seismic performance evaluation of direct-and indirect-hung suspended ceiling systems, *J. Earthquake Eng.* 26 (9) (2022) 4833–4851, <https://doi.org/10.1080/13632469.2020.1845876>. Taylor & Francis.
- [24] R. Retamales, R. Davies, G. Mosqueda, A. Filiatrault, Experimental seismic fragility of cold-formed steel framed gypsum partition walls, *J. Struct. Eng.* 139 (8) (2013) 1285–1293.
- [25] G. Magliulo, C. Petrone, V. Capozzi, G. Maddaloni, P. Lopez, G. Manfredi, Seismic performance evaluation of plasterboard partitions via shake table tests, *Bull. Earthquake Eng.* 12 (4) (2014) 1657–1677.
- [26] X. Wang, E. Pantoli, T. Hutchinson, J. Restrepo, R.L. Wood, M.S. Hoehler, P. Grzesik, F.H. Sesma, Seismic performance of cold-formed steel wall systems in a full-scale building, *J. Struct. Eng.* 141 (10) (2015) 04015014, [https://doi.org/10.1061/\(ASCE\)ST.1943-541X.0001245](https://doi.org/10.1061/(ASCE)ST.1943-541X.0001245).
- [27] C. Jenkins, S. Soroushian, E. Rahmanishamsi, E.M. Maragakis, Experimental fragility analysis of cold-formed steel-framed partition wall systems, *Thin-Walled Struct.* 103 (2016) 115–127.
- [28] B. Schafer, D. Ayhan, J. Leng, P. Liu, D. Padilla-Llano, K. Peterman, M. Stehman, S. Buonopane, M. Eatherton, R. Madsen, et al., Seismic response and engineering of cold-formed steel framed buildings, in: *Structures*, Vol. 8, 2016, pp. 197–212. Elsevier.
- [29] X. Wang, T. Hutchinson, G. Hegemier, S. Gunisetty, P. Kamath, B. Meacham, Earthquake and fire performance of a mid-rise cold-formed steel framed building-test program and test results, rapid release (preliminary), San Diego, CA, 2016 report (ssrp-2016/07).
- [30] C. Petrone, G. Magliulo, G. Manfredi, Shake table tests on standard and innovative temporary partition walls, *Earthquake Eng. Struct. Dyn.* 46 (10) (2017) 1599–1624.
- [31] L. Fiorino, B. Bucciero, R. Landolfo, Evaluation of seismic dynamic behaviour of drywall partitions, façades and ceilings through shake table testing, *Eng. Struct.* 180 (2019) 103–123.
- [32] H.-J. Kim, D.-H. Shin, Shake table test program of cold-formed steel in-plane partition walls, in: *Structures Vol. 30, 2021*, pp. 503–517. Elsevier.
- [33] B. Huang, W. Lu, K.M. Mosalam, Shaking table testing of granite cladding with undercut bolt anchorage, *Eng. Struct.* 171 (2018) 488–499.
- [34] G.S. Johnson, R.E. Sheppard, M.D. Quilici, S.J. Eder, C.R. Scawthorn, Seismic reliability assessment of critical facilities: a handbook, supporting documentation, and model code provisions, in: *Seismic reliability assessment of critical facilities: A handbook, supporting documentation, and model code provisions*, 1999, pp. 384–386.
- [35] N. Achour, Estimation of malfunction of a healthcare facility in case of earthquake, *Hospital (Rio. J.)* 24 (24) (2007) 120.
- [36] M.C. Comerio, J.C. Stallmeyer, R. Smith, N. Makris, D. Konstantinidis, K. Mosalam, T.-H. Lee, J.L. Beck, K.A. Porter, R. Shaikhutdinov, et al., Peer Testbed Study on a Laboratory Building: Exercising Seismic Performance Assessment, 2005. PEER Report 2005/12 (2005/1).
- [37] D. Konstantinidis, N. Makris, Experimental and analytical studies on the response of freestanding laboratory equipment to earthquake shaking, *Earthquake Eng. Struct. Dyn.* 38 (6) (2009) 827–848.
- [38] E. Cosenza, L. Di Sarno, G. Maddaloni, G. Magliulo, C. Petrone, A. Prota, Shake table tests for the seismic fragility evaluation of hospital rooms, *Earthquake Eng. Struct. Dyn.* 44 (1) (2015) 23–40.
- [39] H.H. Hwang, J.-R. Huo, Seismic fragility analysis of electric substation equipment and structures, *Probabilistic Eng. Mech.* 13 (2) (1998) 107–116.
- [40] K. Porter, G. Johnson, R. Sheppard, R. Bachman, Fragility of mechanical, electrical, and plumbing equipment, *Eathquake Spect.* 26 (2) (2010) 451–472.
- [41] H. Son, S. Park, B.-G. Jeon, W.-Y. Jung, J. Choi, B.-S. Ju, Seismic qualification of electrical cabinet using high-fidelity simulation under high frequency earthquakes, *Sustainability* 12 (19) (2020) 8048.
- [42] N.H. Dinh, S.-J. Lee, J.-Y. Kim, K.-K. Choi, Study on seismic performance of a mold transformer through shaking table tests, *Appl. Sci.* 10 (1) (2020) 361.
- [43] S.-J. Wang, Y.-H. Yang, F.-R. Lin, J.-W. Jeng, J.-S. Hwang, Experimental study on seismic performance of mechanical/electrical equipment with vibration isolation systems, *J. Earthquake Eng.* 21 (3) (2017) 439–460.
- [44] H.V. Tran, S.C. Kim, J. Shin, K. Lee, Experimental study of a novel lighting support system reinforced with a pulley friction damper, *J. Building Eng.* 52 (1043) (2022) 85.
- [45] E. ICC, Ac156 Acceptance Criteria for Seismic Certification by Shake-Table Testing of Nonstructural Components, International Code Council Evaluation Service, Country Club Hills, IL, 2011.
- [46] Finley A. Charney, Seismic loads, American Society of Civil Engineers, 2015, <https://doi.org/10.1061/9780784413524>.
- [47] KCSC, Seismic Design Code of Buildings (kds 41 17 00), Ministry of Land, Infrastructure and Transport, Sejong, Korea, 2012.
- [48] U.B. Code, International Code Council, Inc, Falls Church, VA, USA., 2013.
- [49] Shake-table, Testing Method for Seismic Performance Evaluation of Suspended Ceiling, Standard, Korea Construction Engineering Development Collaboratory Management Institute, Gyeonggi-do, ROK, 2021.
- [50] I. 344, Ieee Standard for Seismic Qualification of Equipment for Nuclear Power Generating Stations, 2013.
- [51] F. FEMA, 461-Interim Protocols For Determining Seismic Performance Characteristics of Structural and Nonstructural Components Through Laboratory Testing, federal emergency management agency (fema), document no, Redwood City, CA, 2014.
- [52] R.R.Jr. Craig, A.J. Kurdila, Fundamentals of Structural Dynamics, 2nd, John Wiley & Sons, Inc, New York, USA, 2006.
- [53] Matlab, version 9.8.0 (R2020a), The MathWorks Inc., Natick, Massachusetts, 2020.
- [54] I. Elishakoff, Probabilistic Methods in the Theory of Structures: Strength of Materials, Random Vibrations, and Random Buckling, World Scientific, 2017.
- [55] P. Welch, The use of fast fourier transform for the estimation of power spectra: a method based on time averaging over short, modified periodograms, *IEEE Trans. Audio Elect.* 15 (2) (1967) 70–73.
- [56] O.Jr. Solomon, PSD computations using welch's method, *NASA STI Recon Tech. Rep. N 92 (2358)* (1991) 4.
- [57] G. Housner, P.C. Jennings, Generation of artificial earthquakes, *J. Eng. Mech. Division* 90 (1) (1964) 113–150.
- [58] R. Simmons, femci.gsfc.nasa.gov/random/randomgrms.htmlCalulating grms (root-mean-square acceleration), 1997. <https://femci.gsfc.nasa.gov/random/randomgrms.html>.